2012 IEEE International Conference on Robotics and Automation
RiverCentre, Saint Paul, Minnesota, USA
May 14-18, 2012

Formation Control of Mobile Robots subject to Wheel Slip

Yu Tian and Nilanjan Sarkar, Senior *Member, IEEE*

***Abstract*—Multi-robot formation control has been studied in the literature assuming ideal surface that can provide sufficiently large friction as needed. However, in reality the friction is constrained by terrain characteristic and slip occurs due to insufficient friction. In this paper we investigate the effect of slip on the formation control problem of wheeled mobile robots (WMR). We explicitly model the slip-traction characteristic and integrate it into the WMR dynamics. Input output linearization technique is applied to each WMR such that the entire formation is subject to stable $l-\psi$ control.**

I. Introduction

One of recent research areas on multi-robot cooperative control is formation control [1]-[4]. Various control strategies exist in the literature for such formation control. Generally the distance between the robots, are either kept constant or within a certain range depending on the tasks. As far as the group of robots is concerned, it may either have a real leader, or a virtual leader(s) or no leader at all. In [5] there was a unique leader for the whole group; however each robot had its own direct leader and certain distances were maintained between each leader and its follower robot, while the distances between others were kept in a safe range. In [6], multiple virtual leaders directed the motion of a group. Artificial potential was calculated for each robot to generate pushing or attracting force to keep itself in a certain rage within its nearby robots or virtual leaders. [7]-[9] presented two controllers to maintain the desired separation distance and the relative angle, respectively, between two robots. A single-leader single-follower formation could be maintained by controlling simultaneously the separation and relative angle between them [7][8]. A single-leader double- follower formation could be maintained by controlling the separations between the leader and two followers, respectively [7][8]. WMRs are modeled as single-integrators in [10][11] and as kinematic unicycles in [12][13] for formation control.

When the formation consists of multiple WMRs, slip occurs when they are operated at high speed or on slippery surfaces. In most recent literature, a complete dynamic model of a WMR was established in [14], where slip velocity and traction forces were built into the model. However, they were manipulated to become part of an uncertain term that was ignored in the formation control design. To our knowledge, there has been no work so far that studied multi-WMR formation control subject to wheel slip. Thus the first contribution of the paper is to investigate how a stable formation control algorithm behaves when wheel slip is introduced. In particular, we wanted to understand the impact of slip on formation control. After demonstrating the impact of slip, our second contribution is to design a slip-based controller that can stabilize the formation of the WMR in the presence of wheel slip.

In order to investigate the effect of slip on formation control of WMRs, we chose one well-known algorithm namely, the leader-follower formation control [7], among the several published formation control algorithms. In this work, to demonstrate the concept, we chose three WMRs in the group. The leader is governed by a path following control and the other two followers are governed by $l-\psi$ control [8][15][16]. Briefly, the $l-\psi$ control is for a follower WMR to preserve the desired inter-distance l and the relative angle ψ from its leader. It has been extensively used in formation control literature and is thus chosen as our target strategy for formation control. We apply input-output linearization in this paper to derive the $l-\psi$ control law for the follower WMRs when outputs l and ψ are chosen.

This paper is organized as follows. In Section II the importance of slip consideration is discussed for multi-WMR formation control problem. In Section III the WMR model with wheel slip and the model of the traction force between the wheels and the surfaces are introduced. The model is then used to develop a slip-based controller that is used in the multi-WMR formation control subject to slip in Section IV. In Section V, we present simulation results to show the multi-WMR formation control behavior subject to slip. We summarize our contributions in Section VI.

II. Importance of Slip Consideration in Formation Control

In this section, we demonstrate by examples that, for a stable formation under $l-\psi$ control, if slip occurs due to insufficient friction the formation will become unstable. Let us first consider an example of the formation control assuming no slip. This example uses the model in [17] where there is no slip. The leader WMR starts at point $[x_0, y_0, \phi_0] = [0,0,0]$ and follows an *L*-shape path with an initial speed of 2.5m/s, which is also the desired speed. The *L*-shape path consists of straight line $L_1=\{(x,y)|y=0,x<10\}$ and $L_2=\{(x,y)|x=10,y>=0\}$. The other two follower WMRs start from [-4,4,0], [-4,-4,0] and follow the leader while preserving the desired inter-distance of 5m and the relative angles of $\pi/4$ and $3\pi/4$ radians from the leader. The

Yu Tian is with the Department of Mechanical Engineering, Vanderbilt University, Nashville, TN, 37235 USA (e-mail: ytian.xp@gmail.com)

Nilanjan Sarkar is with the Department of Mechanical Engineering, Vanderbilt University, Nashville, TN, 37235 USA (e-mail: nilanjan.sarkar@vanderbilt.edu).

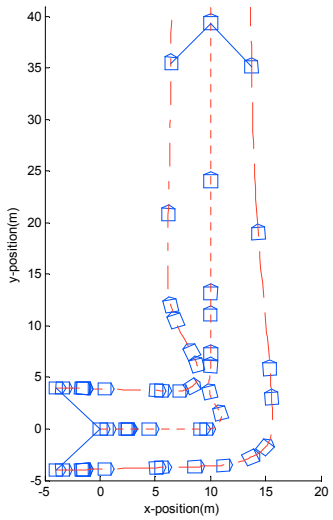

Fig. 1 WMR formation in example 1

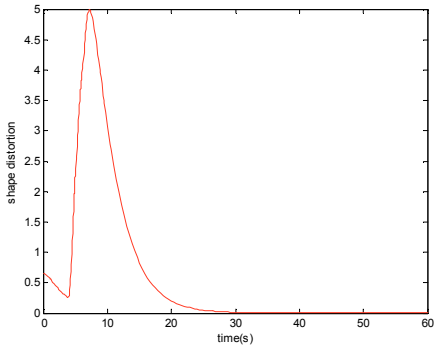

Fig. 2 Shape distortion in example 1

controller for the leader is a path following control. Path following control is to control a robot to follow a given path at a given speed. The controller for the follower WMRs is $l-\psi$ controller. The input-output linearization technique in Section IV shows that, when we take second order derivative of the outputs l and ψ, the torque input appears. Then the transfer functions for the desired l and ψ between the inputs and outputs in the linearized close-loop model are

$$H_{dis}(s)=\frac{k_{pd}}{s^2+k_{vd}s+k_{pd}}, \qquad (1)$$

$$H_{ang}(s)=\frac{k_{pa}}{s^2+k_{va}s+k_{pa}}$$

and we choose the control gains k_{pd}=0.5, k_{vd}=2 and k_{pa}=0.5, k_{va}=2, respectively.

As an example of traversing a path with a given formation, we choose an L-shape path that is followed by three WMRs with a given $l-\psi$ formation. In Fig. 1 we observe the path of the three WMRs following an *L*-shape path while preserving a triangular formation. As expected, during the sharp bend, the formation is perturbed but is soon recovered since the formation control algorithm is stable. In order to quantitatively capture the shape distortion of the formation,

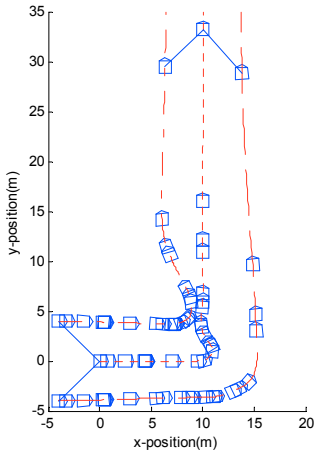

Fig. 3 WMR formation in example 2

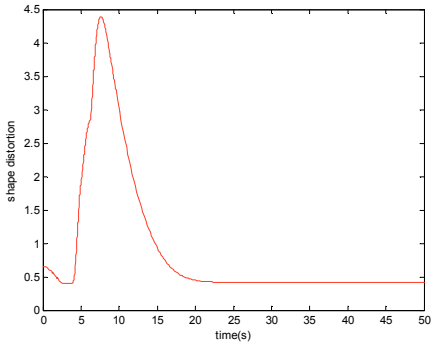

Fig. 4 Shape distortion in example 2

we use the concept of Procrustes distance [18]. The Procrustes distance is defined based on the following definitions.

Definition 1 [18] The **configuration** is the set of landmarks on a particular object. The **configuration matrix** X is the $k\times m$ matrix of the Cartesian coordinates of the k landmarks in m dimensions. An $m\times m$ rotation matrix satisfies $\Gamma^T\Gamma=\Gamma\Gamma^T=I_m$ and $|\Gamma|=1$. The set of all m×m rotation matrices is known as the Special Orthogonal group SO(m). If a $k\times k$ matrix has its first row with elements equal to $k^{-1/2}$ and the remaining rows are orthogonal to this first row, this matrix is **Helmert matrix**. Let Helmert matrix minus its first row be **Helmert sub-matrix**. The jth row of the Helmert sub-matrix H is given by

$$(h_j,...,h_j,-jh_j,0,...,0),\quad h_j=-\{j(j+1)\}^{-1/2}$$

and so the jth row consists of h_j repeated j times, followed by jh_j and then k-j-1 zeros, j=1,…,k-1.

For k=3, the full Helmert matrix and submatrix are

$$H^F=\begin{bmatrix}1/\sqrt{3} & 1/\sqrt{3} & 1/\sqrt{3}\\ -1/\sqrt{2} & 1/\sqrt{2} & 0\\ -1/\sqrt{6} & -1/\sqrt{6} & 2/\sqrt{6}\end{bmatrix},\quad H=\begin{bmatrix}-1/\sqrt{2} & 1/\sqrt{2} & 0\\ -1/\sqrt{6} & -1/\sqrt{6} & 2/\sqrt{6}\end{bmatrix} \qquad (2)$$

Definition 2 [13] The size-and-shape of a configuration matrix X is all the geometrical information about X that is invariant under location and rotation (rigid-body trans-formations), and this can be represented by the set $[X]_S$ given

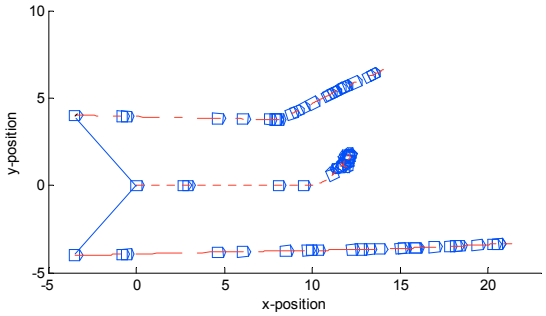

Fig. 5 WMR formation in example 3

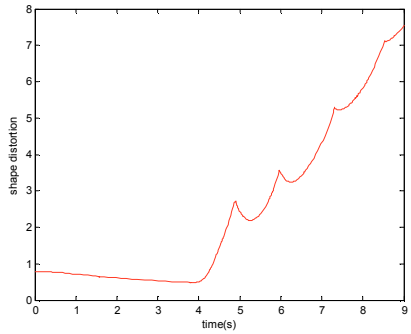

Fig. 6 Shape distortion in example 3

by $[X]_S = \{X_H\Gamma : \Gamma \in SO(m)\}$, where X_H=HX. The Procrustes distance d_P is obtained by matching the Helmert coordinates X_{H1} and X_{H2} of X_1 and X_2 as closely as possible over rotations. Thus $d_P(X_1, X_2) = \inf_{\Gamma \in SO(m)} \|X_{H1} - X_{H2}\Gamma\|$.

This Procrustes distance represents shape distortion in our formation control task, where X_1 is the configuration matrix for three WMRs in the actual formation, and X_2 is the configuration matrix for three WMRs in the desired formation. Both X_1 and X_2 are 3×3 matrices. Fig. 2 shows the shape distortion as the team follows the L-shaped path trying to preserve the desired formation. As can be observed, initially there was a shape distortion (we chose that way) from which the team was trying to recover (up until approximately 4s) when the leader takes the sharp turn. The shape distortion increases quickly. However, since this is a stable formation control algorithm, the team converges to their desired shape and the shape distortion goes to zero.

Now we demonstrate that the formation is still stable if small amount of slip occurs. In this case, everything is the same as the previous example except that each WMR has a slip-traction model. We use the model in Section III for this example. The friction coefficient chosen for this simulation is 0.7. The triangular formation evolution and shape distortion during the *L*-shape path following can be observed in Fig. 3 and Fig. 4. Because the amount of slip is small, sufficient traction can be provided for stable formation control. However, the actual formation cannot converge to the desired formation because the controller does not have the knowledge of slip thus cannot compensate slip.

Next we demonstrate that this stable formation becomes unstable if large amount of slip occurs. In this case, everything is the same as the previous example except that the friction coefficient chosen for this simulation is 0.3. The triangular formation evolution and shape distortion during the *L*-shape path following can be observed in Fig. 5 and Fig. 6. Because of slip, the leader cannot take a sharp turn and as a result, the formation control becomes unstable quickly.

Thus it can be seen that formation control algorithm is sensitive to slip, which is intuitive from a physical understanding. We argue in this paper that a realistic formation control algorithm for WMRs should consider wheel slip. We develop such a formulation in the next section.

III. Dynamic WMR Model Subject to Wheel Slip

There is no literature to our knowledge that has considered wheel slip in formation control of WMRs. However, there has been some important work in modeling and control of wheel slip for individual WMR. In [19] anti-slip factor was introduced to represent the amount of slip. In [20-21] slip is introduced into kinematic WMR modeling and control. In [22][23] longitudinal slip was considered in WMR. In [24-26] the traction forces were introduced into WMR modeling and approximated to be linearly dependent on slips. In this paper, we model wheel slip in the overall nonholonomic WMR dynamics and exploit the slip and traction force such that the maneuverability of the WMR can be improved for formation control.

The WMR subject to wheel slip is modeled as in Fig. 7, where P_c is the center of mass of the WMR, P_0 is the center of the wheel shaft, d is the distance from center of mass P_c to P_0, b is the distance from the center of each wheel to P_0. F_1 and F_2 are the longitudinal traction forces for $wheel_1$ and $wheel_2$, respectively. F_3 is the total lateral traction force. Note that a dynamic model needs to be studied in order to take into account the effect of slip on the WMR. The equations for the dynamic WMR model are derived from Newton's Law as shown in (3).

$$\begin{cases} M\ddot{x}_c = (F_1 + F_2)\cos\phi - F_3\sin\phi \\ M\ddot{y}_c = (F_1 + F_2)\sin\phi + F_3\cos\phi \\ I\ddot{\phi} = (F_1 - F_2)b - F_3 d \end{cases} \quad (3.a)$$

$$\begin{cases} I_w\ddot{\theta}_1 = \tau_1 - F_1 r \\ I_w\ddot{\theta}_2 = \tau_2 - F_2 r \end{cases} \quad (3.b)$$

where M is the mass and I is its moment of inertia of the WMR, respectively, I_w is the moment of inertia of each wheel about the wheel axis, r is the wheel radius, ϕ is the orientation of the WMR, θ_i is the angular displacement of the i-th wheel, and τ_i is the wheel torque applied to the i-th wheel. Equation (3.a) represents the entire WMR dynamics in the plane while (3.b) represents the spinning dynamics of the wheels.

The lateral and longitudinal traction forces are functions of slip angle (sa) and slip ratio (sr), respectively, and are modeled following the *Pacejka* model [27] in the literature. The slip angle and the slip ratio are defined as

$$sr_i = \frac{r\dot{\theta}_i - v_i}{v_i},\ sa = \tan^{-1}(\frac{\dot{\eta}}{v}), \quad (4)$$

where v_i is the longitudinal speed of the center of the i-th wheel, $v = (v_1 + v_2)/2$ is the forward speed, $\dot{\eta}$ is the lateral speed of the center of each wheel. They satisfy the following nonholonomic constraints [28]

$$v_1 = \dot{x}_c \cos\phi + \dot{y}_c \sin\phi + b\dot{\phi} \quad (5)$$

$$v_2 = \dot{x}_c \cos\phi + \dot{y}_c \sin\phi - b\dot{\phi} \quad (6)$$

$$\dot{\eta} = \dot{y}_c \cos\phi - \dot{x}_c \sin\phi - d\dot{\phi} \quad (7)$$

where (x_c, y_c) is the coordinates of P_c.

Note that, unlike classical nonholonomic constraints of WMR, the above constraints allow both longitudinal and lateral slips.

The traction force between a wheel and a surface is modeled as [27]

$$F = K_1 \sin\left(K_2 \tan^{-1}\left(SK_3 + K_4\left(\tan^{-1}(SK_3) - SK_3\right)\right)\right) + S_v, \quad (8)$$

where S is a function of slip angle for lateral traction force and slip ratio for longitudinal traction force. All other variables K_i, i=1,…,4 and S_v are constants and are determined from the curve fitting process of the empirical data. K_1 is proportional to friction coefficient. Fig. 8 shows an example of lateral traction forces with friction coefficient 0.7 and 0.3, respectively. The example of longitudinal traction force is omitted as its profile is similar to that of the lateral traction force.

Since F_i (i=1,2) is a functions of sr_i(i=1,2), sr_i(i=1,2) is a function of $\dot{\theta}_i$ (i=1,2) and $\ddot{\theta}_i$ (i=1,2) is a function of τ_i (i=1,2), $\dot{F}_i$ (i=1,2) becomes a function of τ_i (i=1,2), as shown in (9). Thus after taking the derivative of (3.a), it becomes a third order system with τ_i as the input.

IV. Multi-WMR Formation Control Subject to Slip

4.1 Dynamic Path Following Control for the Leader

We approach the dynamic path following control [17] problem of the leader by applying input-output linearization technique. Define a look-ahead point P_l on the robot as in Fig. 7. The dynamic path following is to maintain this point on the desired path and maintain its forward velocity, i.e., speed of this point along moving direction, at the desired velocity. The coordinates of P_l of the leader are given by

$$\begin{aligned} x_l &= x_c + L\cos\phi \\ y_l &= y_c + L\sin\phi \end{aligned}, \quad (10)$$

where L is the distance from P_l to P_c.

Define the output equation for P_l as $h = [h_1(q) \quad h_2(\dot{q})]^T$ where h_1 is the distance of the leader from the desired path, h_2 is the leader's forward velocity and $q = [x_c, y_c, \phi]^T$. Although dynamic path following can be applied to both straight lines and circular paths [17], we take the straight line path as an example.

For straight line paths, $h_1(q)$ becomes

$$h_1(q) = \frac{|C_1 x_l + C_2 y_l + C_3|}{\sqrt{C_1^2 + C_2^2}}, \quad (11)$$

where all $C_i, i = 1,2,3$ are constants used to describe the straight-line. From (11), we see that the shortest distance between the look-ahead point and the path can be taken as h_1. The forward velocity of the WMR can be written as

$$h_2(\dot{q}) = \dot{x}_c \cos\phi + \dot{y}_c \sin\phi \ . \quad (12)$$

Now, we proceed to develop a nonlinear controller based on the input-output linearization technique such that

$$\begin{aligned} \dot{h}_1 &= \frac{\partial h_1}{\partial q}\dot{q} = J_{h_1}\dot{q},\ \ddot{h}_1 = \frac{\partial^2 J_{h_1}}{\partial q^2}\dot{q}^3 + 3\frac{\partial J_{h_1}}{\partial q}\dot{q}\ddot{q} + J_{h_1}\ddot{q} \\ \dot{h}_2 &= \frac{\partial h_2}{\partial \dot{q}}\ddot{q} = J_{h_2}\ddot{q},\ \ddot{h}_2 = \frac{\partial J_{h_2}}{\partial \dot{q}}\ddot{q}^2 + J_{h_2}\ddot{q} \end{aligned}. \quad (13)$$

As an example, for the straight-line path,

$$J_{h_1} = \frac{1}{\sqrt{C_1^2 + C_2^2}}[C_1 \quad C_2 \quad C_2 L\cos\phi - C_1 L\sin\phi \quad 0 \quad 0 \quad 0 \quad 0] \text{ and}$$

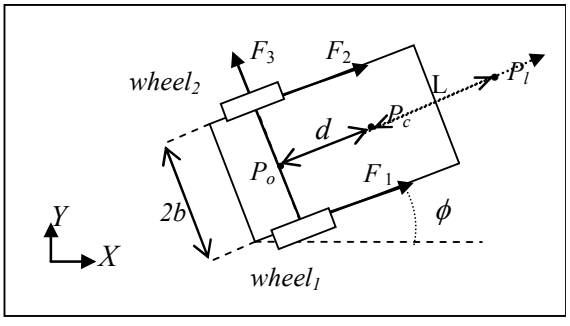

Fig. 7 WMR model subject to wheel slip.

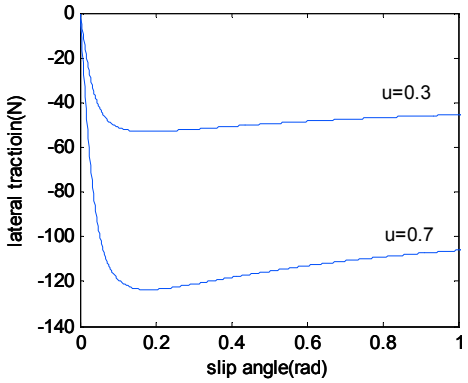

Fig. 8 Lateral traction for friction coefficients 0.7 and 0.3.

$$\dot{F}_i = \frac{K_1 K_2 \cos(K_2 \tan^{-1}(K_3 sr_i + K_4(\tan^{-1}(K_3 sr_i) - K_3 sr_i)))(K_3 + K_4(\frac{K_3}{1 + K_3^2 sr_i^2} - K_3))}{1 + (K_3 sr_i + K_4(\tan^{-1}(K_3 sr_i) - K_3 sr_i))^2} \frac{rv_i\tau_i - F_i r^2 v_i - rI_w\dot{\theta}_i\dot{v}_i}{I_w v_i^2} \quad (9)$$

$J_{h_2} = [\cos\phi \quad \sin\phi \quad 0]$. $J_{h_i} = \frac{\partial h_i}{\partial q}$ (i=1,2) is known as the *Jacobian* matrix and we can use them to compute the decoupling matrix, Φ as follows,

$$\Phi = \begin{bmatrix} J_{h_1} \\ J_{h_2} \end{bmatrix}. \tag{14}$$

We utilize the decoupling matrix to establish the input-output feedback linearization as shown below,

$$\begin{bmatrix} \ddot{h}_1 \\ \ddot{h}_2 \end{bmatrix} = \begin{bmatrix} \dot{J}_{h_1} \\ 0 \end{bmatrix} \dot{q} + \left(\begin{bmatrix} J_{h_1} \\ 0 \end{bmatrix} + \dot{\Phi} \right) \ddot{q} + \Phi \ddot{q} \tag{15}$$

.

If we represent (15) in the form of $[\dddot{h}_1 \quad \ddot{h}_2]^T = U + V\ddot{q}$, where $\ddot{q}$ is a function of $\dot{F}$ as in (3) and $\dot{F}$ is a function of wheel torque as in (9), we can have dynamics between input and output as $[\dddot{h}_1 \quad \ddot{h}_2]^T = P + Q\tau$ where τ is torque input vector. Thus the slip-traction characteristics are included within the control dynamics of the WMR. If we design a new control input as $u_d = P + Q\tau$, the system is linearized to be $[\dddot{h}_1 \quad \ddot{h}_2]^T = u_d$, for which we can design a linear controller as,

$$u_d = [\dddot{h}_1 \quad \ddot{h}_2]^T_{desired} + K_i[\ddot{e}_1 \quad \dot{e}_2]^T + K_v[\dot{e}_1 \quad e_2]^T + K_p[e_1 \quad 0]^T \tag{16}$$

where $e_i = h_{i\_desired} - h_{i\_actual}$ and K_i, K_v and K_p are control gains for the linearized system. Then the torque input to the original nonlinear system becomes

$$\tau = Q^{-1}(u_d - P) . \tag{17}$$

We call this controller a slip-sensitive controller.

4.2 Follower Control

For each follower in the formation, its distance l and orientation ψ from its direct leader are controlled to maintain at desired values. Define the output as $h_f = [h_{f1}(q) \quad h_{f2}(\dot{q})]^T$

where h_{f1} is the distance of the follower from its leader,

$$h_{f1}(q) = \sqrt{(x_{l(follower)} - x_{l(leader)})^2 + (y_{l(follower)} - y_{l(leader)})^2} \tag{18}$$

and h_{f2} is the orientation of the l vector relative to the leader's orientation,

$$h_{f2}(q) = \tan^{-1}\left(\frac{y_{l(follower)} - y_{l(leader)}}{x_{l(follower)} - x_{l(leader)}}\right) - \phi_{leader} \tag{19}$$

and x_l and y_l are defined in (10) for both leader and follower. Then the input-output linearization technique in Section 4.1 can be applied and a linear control law can be derived for each follower, which is omitted in this section. The input to the original nonlinear system becomes $\tau = Q_f^{-1}(u_d - P_f)$. (20)

Note that the slip-sensitive controller presented here assumes the knowledge of slip to develop the controller for formation control in simulation. In real world, slip will not be known a priori. It will be either measured or estimated [29-33].

V. Simulation Results

In this simulation, we show that when the slip-sensitive controller is used, it is possible to stabilize the formation control algorithm that did not work when the terrain was slippery. We consider everything to be the same as in the second example in Section II except for the controllers of the WMRs. The transfer functions for desired l and ψ in the linearized close-loop model are

$$H_{dis}(s) = \frac{K_{pd}}{s^3 + K_{id}s^2 + K_{vd}s + K_{pd}}, \tag{21}$$

$$H_{ang}(s) = \frac{K_{pa}}{s^3 + K_{ia}s^2 + K_{va}s + K_{pa}}$$

and the control gains K_{pd}=50, K_{vd}=200.5, K_{id}=102 and K_{pa}=50, K_{va}=200.5, K_{ia}=102, respectively. These control gains are derived by letting the frequency response of the close-loop model in this case same as that in the first example in Section II. To do so, we need to find a number a>>1 such that

$$(s+a)(s^2 + k_{vd}s + k_{pd}) = s^3 + K_{id}s^2 + K_{vd}s + K_{pd}.$$

$$(s+a)(s^2 + k_{va}s + k_{pa}) = s^3 + K_{ia}s^2 + K_{va}s + K_{pa}$$

We set a=100, hence K_{pd}=a*k_{pd}=50, K_{vd}=k_{vd}*a+k_{pd}=200.5, K_{id}=a+k_{vd}=102, K_{pa}=a*k_{pa}=50, K_{va}=k_{va}*a+k_{pa}=200.5, K_{ia}=a+k_{va}=102.

The formation evolution and shape distortion during L-shape path following can be observed in Fig. 9 and Fig. 10. Note that when the slip is considered in the controller, slip is compensated, the formation converges to the desired shape and the shape distortion goes to zero.

VI. Conclusions

This is the first time to our knowledge that mobile robot formation control has been studied in the presence of wheel slip. The first contribution of this paper is to show that a stable formation can become unstable if the slip is significant. We then proceed to develop a slip-sensitive controller that can stabilize the formation even when slip is significant.

Note that the developed slip-sensitive controller

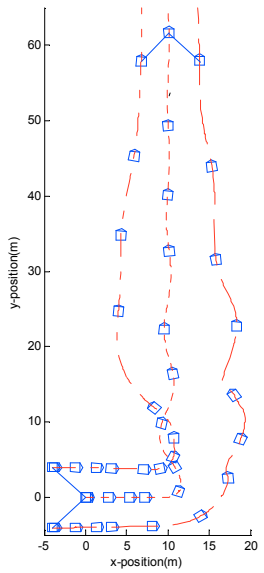

Fig. 9 WMR formation

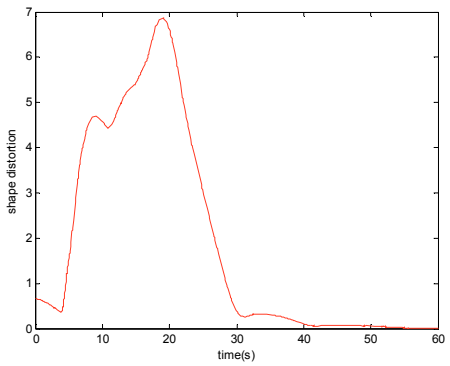

Fig. 10 Shape distortion

compensates for the slip as much as possible, however, it cannot guarantee that it can achieve the desired forward speed under large slip. The forward speed is limited by the physics of slip-traction characteristics, and an arbitrarily high speed cannot be achieved if there is not enough traction. The formation control algorithms that do not consider slip cannot decide at what speed they will not be able to follow the formation. Our presented approach will be aware of speed limitation for a given slip-traction characteristic and will be able to adjust speed to keep the formation stable. In the future, we will develop a robust outer control loop to compensate for modeling uncertainty that may impact input-output linearization.

REFERENCES

[1] Y. Chen and Z. Wang, "Formation Control: A Review and A New Consideration," *IEEE International Conference on Intelligent Robots and Systems,* Aug. 2005, pp. 3181-3186.

[2] F. Giulietti, L. Pollini and M. Innocenti, "Autonomous Formation Flight," *IEEE Control Systems Magazine*, vol. 20, issue 6, Dec. 2000, pp. 33-44.

[3] D. Swaroop J. K. Hedrick and S. B. Choi, "Direct Adaptive Longitudinal Control of Vehicle Platoons," *IEEE Trans. On Vehicular Technology,* vol. 50, No. 1, Jan. 2001, pp. 150-161.

[4] M. C. De Gennaro and A. Jadbabaie, "Formation Control for a Cooperative Multi-Agent System using Decentralized Navigation Functions", *Proc. of American Control Conference*, Minneapolis, Minnesota, USA, Jun. 14-16, 2006.

[5] G. A. S. Pereira, A. K. Das, V. Kumar and M. F. M. Campos, "Formation Control with Configuration Space Constraints," *Proc. of IEEE International Conference on Robots and Systems,* vol. 3, Oct. 2003, pp. 2755-2760.

[6] N. E. Leonard and E. Fiorelli, "Virtual Leaders, Artificial Potentials and Coordinated Control of Groups," *Proc. of IEEE International Conference on Decision and Control,* vol. 3, 4-7, Dec. 2001, pp. 2968-2973.

[7] J. P. Desai, "Motion Planning and Control of Cooperative Robotic Systems," Ph.D. dissertation, Dept. Mech. Eng. and Appl. Mech, Univ. of Pennsylvania, Philadelphia, MD, 1998.

[8] J. P. Desai, J. P. Ostrowski and V. Kumar, "Modeling and Control of Formation of Nonholonomic Mobile Robots," *IEEE Trans. Robotics and Automation,* vol. 17, No. 6, Dec. 2001.

[9] R. Fierro, A. K. Das, V. kumar and J. P. Ostrowski, "Hybrid Control of Formations of Robots," *Proc. of IEEE International Conference on Robotics and Automation,* vol. 1, Seoul, Korea, May. 2001, pp. 151-162.

[10] Kwang-Kyo Oh and Hyo-Sung Ahn, "Distance-based Formation Control Using Euclidean Distance Dynamics Matrix: Three-agent Case", *IEEE American Control Conference*, San Francisco, USA, June 2011, pp. 4810-4815.

[11] Jing Guo, Zhiyun Li, Ming Cao and Gangfeng Yan, "Adaptive Leader-Follower Formation Control for Autonomous Mobile Robots", *IEEE American Control Conference*, Baltimore, USA, June 2010, pp. 6822-6827.

[12] Ke-Cai Cao, "Formation Control of Multiple Nonholonomic Mobile Robots Based on Cascade Design", *IEEE Conference on Decision and Control*, Shanghai, China, December, 2009, pp. 8340-8344.

[13] Gayan W. Gamage, George K.I. Mann and Raymond G. Gosine, "Leader follower based formation control strategies for nonholonomic mobile robots: Design, Implementation and Experimental Validation",

[14] Celso De La Cruz and Ricardo Carelli, "Dynamic model based formation control and obstacle avoidance of multi-robot systems", *Robotica*, Vol. 26, Issue 03, 2008, pp. 345-356.

[15] Travis Dierks and S. Jagannathan, "Control of Nonholonomic Mobile Robot Formations: Backstepping Kinematics into Dynamics", *IEEE International Conference on Control Applications*, 2007, pp. 94-99.

[16] S. A. Panimadai Ramaswamy and S. N. Balakrishnan, "Formation Control of Car-Like Mobile Robots: A Lyapunov Function Based Approach", *2008 American Control Conference*, pp. 657-662.

[17] Sarkar N., Yun X., "Control of mechanical systems with rolling constraints: Application to the dynamic control of mobile robots", *Int. Journal of Robotics Research*, Vol. 31, 1994, pp. 55-69.

[18] Ian L. Dryden and Kanti V. Mardia, *Statistical Shape Analysis*, John Wiley & Sons, West Sussex, England, 1998.

[19] Lin W.-S., Chang L.-H., Yang P.-C., "Adaptive critic anti-slip control of wheeled autonomous robot**"**, Control Theory & Applications, IET, Vol. 1, Issue 1, 2007, pp. 51-57.

[20] Tarokh M., McDermott G.J., "Kinematics modeling and analyses of articulated rover", *IEEE Trans. on Robotics*, Vol. 21, No.4, 2005, pp. 539-553.

[21] Dixon W.E., Dawson D.M., Zergeroglu E., "Robust control of a mobile robot system with kinematic disturbance", *IEEE Int. Conference on Control Applications*, 2000, pp. 437-442.

[22] Balakrishna R. and Ghosal A., "Modeling of slip for wheeled mobile robot", *IEEE Trans. on Robotics and Automation*, Vol. 11, No. 1, 1995, pp. 126-132.

[23] Stonier D., Hyoung C. Se-, Sung-Lok C., Kuppuswamy N.S., Jong-Hwan K., "Nonlinear slip dynamics for an omni-wheel mobile robot platform", *IEEE Int. Conf. on Robotics and Automation*, 2007, pp. 2367-2372.

[24] Motte I., Campion I., "A slow manifold approach for the control of mobile robots not satisfying the kinematic constraints", *IEEE Trans. on Robotics and Automation*, Vol. 16, No. 6, 2000, pp. 875-880.

[25] Jung S., Hsia T.C., "Explicit lateral force control of an autonomous mobile robot with slip", *IEEE/RSJ Int. Conf. on Intelligent Robots and Systems*, IROS 2005, pp. 388-393.

[26] Jeren Ploeg, Hanno E. Schouten and Henk Nijmeijer, "Control Design for a Mobile Robot Including Tire Behavior", *2008 IEEE Intelligent Vehicles Symposium*, Eindhoven, The Netherlands, June 4-6, 2008, pp. 240-245.

[27] H. B. Pacejka and E. Bakker, "The Magic Formula Tyre Model", *Vehicle System Dynamics*, vol. 21, 1992, pp. 1-18.

[28] N. Sidek and N. Sarkar, "Dynamic Modeling and Control of Nonholonomic Mobile Robot with Lateral Slip", *IEEE International Conference on Systems*, ICONS 2008, pp. 35-40.

[29] Ward C.C., Iagnemma K., "Model-based wheel slip detection for outdoor mobile robots", *IEEE Int. Conf. on Robotics and Automation*, 2007, pp. 2724-2729.

[30] Angelova A., Matthies L., Helmick D.M., Sibley G., Perona P., "Learning to predict slip for ground robots", *Proc. of IEEE Int. Conf. on Robotics and Automation*, 2006, pp. 3324-3331.

[31] Seyr M., Jakubek S., "Proprioceptive navigation, slip Estimation and slip control for autonomous wheeled mobile robot", *IEEE Conf. on Robotics, Automation and Mechatronics*, Dec. 2006, pp. 1-6.

[32] Politis Z., Probert Smith P.J. (2001), Classification of textured surfaces for robot navigation using continuous transmission frequency-modulated sonar signatures, *Int. Journal of Robotics Research*, 20(2), pp. 107-128.

[33] Vandapel N., Huber D.F., Kapuriac A., Hebert M. (2004), Natural terrain classification using 3-D ladar data, *Proc. of IEEE Int. Conf. on Robotics and Automation*, 26, pp. 5117 – 5122.